ZnO(101¯0) is unstable in moderate pressures of water

Wenzel, S.; Groot, I.M.N.

Surface Science 715 (2022) 121940

Contents lists available at ScienceDirect

Surface Science

journal homepage: www.elsevier.com/locate/susc

ZnO($10\bar{1}0$) is unstable in moderate pressures of water

Sabine Wenzel *, Irene M.N. Groot

Leiden Institute of Chemistry, PO box 9502, RA Leiden 2300, The Netherlands

ARTICLE INFO

Keywords:
ZnO
Single crystal
Scanning tunneling microscopy
In situ
Methanol steam reforming
Water

ABSTRACT

A ZnO($10\bar{1}0$) single crystal was investigated using in situ scanning tunneling microscopy and X-ray photoelectron spectroscopy. In roughly 1 mbar water the surface roughens within minutes. Hereby, the formation of (0001)- or ($000\bar{1}$)-type steps is favored over the formation of ($1\bar{2}10$)-type steps. The roughened surface is stable in ultra-high vacuum and does not exhibit a different amount of hydroxylation or adsorbed water compared to the as-prepared surface. The speed of the roughening is related to the total volume of water supplied to the surface rather than the water pressure.

1. Introduction

Methanol is interesting as an energy-storage material. It can be produced from renewable sources [1], is biodegradable [2], and, being liquid at room temperature [3], it can be stored more easily and safely than hydrogen. In order to harvest the energy, methanol can be converted to hydrogen via the methanol steam reforming reaction:

$$CH_3OH + H_2O \rightarrow 3\ H_2 + CO_2 \quad (1)$$

Carbon monoxide forms as a side product to the methanol steam reforming reaction [4]. This is the main challenge in converting the hydrogen further to electricity using a fuel cell. The platinum anode of hydrogen fuel cells is poisoned by a few parts per million of CO [5]. Therefore, a methanol steam reforming catalyst with a high selectivity towards CO_2 instead of CO is needed. The industrially-used catalyst for methanol synthesis Cu-ZnO/Al_2O_3 also shows significant activity for methanol steam reforming and has been researched extensively [6–8].

Zinc oxide alone is active itself and relevant for the CO_2 selectivity of the methanol steam reforming catalyst [9,10]. Studies on zinc oxide single crystals of different faces are aiming at understanding its role at the atomic level. The interaction of ZnO($10\bar{1}0$) with methanol [11–13], water [14,15], atomic hydrogen [16], CO [17,18] and CO_2 [19,20] has been studied extensively under ultra-high vacuum (UHV) conditions. Among these studies are microscopy measurements as well as diffraction, desorption spectroscopy, and theoretical studies. Spectroscopy measurements on the interaction with water have been conducted under near-ambient pressure conditions [21]. However, to our knowledge, there is no microscopy study showing the surface under these conditions. The ReactorSTM setup [22] allows for combining controlled UHV preparation with nanometer-scale imaging in the mbar range of water. In the following we present ex situ as well as in situ imaging of ZnO($10\bar{1}0$) in moderate pressures of water, and investigate the role of surface hydroxylation with X-ray photoelectron spectroscopy.

2. Materials and methods

The experimental setup has been described in detail by Herbschleb et al. [22]. In short, the scanning tunneling microscope (STM) can be used in UHV (base pressure $< 10^{-9}$ mbar) as well as in up to 6 bar of gases. This is possible in a flow reactor cell of about 0.05 ml volume, which is closed off from the rest of the vacuum chamber by the sample, the STM body, and a Kalrez© seal. The video-rate control electronics were described by Rost et al. [23] and the control software is Camera 6.1 [24]. A cut platinum iridium wire (Pt90/Ir10, 0.25 mm) is used as the STM tip. During a scan on a cleaned Au(111) single crystal the tip can be prepared by tip pulsing and the distance and height are calibrated. The STM images are processed in WSxM [25]. The gas used here is argon 5.0 from Westfalen, which contains 3 ppm water [26]. However, due to the design of the gas mixing system a higher amount of water is present. A measurement of the water content is described in the supplemental information and reveals a water content on the order of 1 mbar water when filling the reactor to 1 bar of any gas.

The ZnO($10\bar{1}0$) single crystal is purchased from SPL. The surface is prepared by cycles of 20 min sputtering in $1 \cdot 10^{-6}$ mbar of argon with an acceleration voltage of 1.4 kV resulting in a sample current of 4 μA on a surface area of 0.5 cm^2 followed by 20 min of annealing to 795 K in

* Corresponding author.
E-mail address: s.wenzel@lic.leidenuniv.nl (S. Wenzel).

https://doi.org/10.1016/j.susc.2021.121940
Received 9 July 2021; Received in revised form 6 September 2021; Accepted 7 September 2021
Available online 10 September 2021

UHV. A K-type thermocouple consisting of two 0.125 mm thick wires is spot-welded to a plate holding the sample in place. The temperature read-out is made as accurate as possible by heating up and cooling down slowly (at maximum 1 K/s). The annealing temperature measured is likely underestimated by up to about 120 K for technical reasons [27].

Complementary UHV techniques available in the same setup are low-energy electron diffraction (LEED) with an Omicron SpectaLEED and NG LEED S control unit, and X-ray photoelectron spectroscopy (XPS) with a VG Microtech dual anode X-ray source and a Clam 2 analyzer. These techniques can be performed in $< 5 \cdot 10^{-9}$ mbar before and after the in situ microscopy without exposing the sample to air in between. The X-ray photoelectron oxygen 1s peaks were fitted using CasaXPS 2.3.19. A zinc Auger peak with a tail towards high binding energies partly overlaps with the oxygen peak such that the background on its low binding energy side appears too high. Therefore, the oxygen 1s peak stemming from the ZnO itself, which we will refer to as the bulk oxygen peak, is likely underestimated in comparison to any other oxygen 1s peaks which are shifted to higher binding energies. We identify a peak at + 1.5 eV with respect to the bulk peak as adsorbed OH and a peak with a shift of + 3.5 eV as molecularly adsorbed water on top of the hydroxylated surface [28]. The shifts of these peaks were fixed during fitting and the full width half maximum of all peaks was constrained. A linear background subtraction was used and Gaussian-Lorentzian product functions with a ratio of 1:1 gave the most satisfactory fit. (Two example fits are given in the results section.)

The relative peak areas of the OH and the H_2O peaks, A_{OH}/A_{total} and A_{H_2O}/A_{total} respectively, with $A_{total} = A_{bulk} + A_{OH} + A_{H_2O}$, are used as a measure for the amount of hydroxylation and adsorbed molecular water. In order to minimize beam effects on the XPS results the O 1s spectra were measured immediately after moving the sample into the X-ray beam. A comparison of the first and last of 30 sweeps of the oxygen area for one example measurement (after argon exposure for 10 min at 300 K) reveals no significant change of the signal on the time scale of the XPS measurement. All relative peak areas given in Section 3.3 are derived from the average of all sweeps for each measurement to improve the signal-to-noise ratio and to keep the measurements in the different situations comparable.

Similarly, the sample is only moved in front of the electron gun of the LEED right before a measurement to prevent an influence of the beam. Although an exposure of a couple of minutes is necessary until the settings are optimized to see the water overlayer, the LEED pattern did not change anymore afterwards on the time scale of an hour.

3. Results and discussion

3.1. As-prepared ZnO($10\bar{1}0$) in UHV

Fig. 1 (a) shows the ZnO($10\bar{1}0$) surface at 400 K after about 100 cleaning cycles. 10-nm to 40-nm-wide flat terraces are visible in the large-scale image in (a) with two types of step edges orthogonal to each other. The step heights in this image measure as (0.30 ± 0.04) nm which is in agreement with the value of 0.281 nm expected from the crystal structure [29]. In the smaller-scale image in (b) regular parallel lines are visible. Their distance, averaged over measurements on multiple images, is (0.59 ± 0.09) nm, which can be identified as the size of the unit cell in the [0001] direction by comparison to the value of 0.521 nm based on the crystal structure. The higher lines can be attributed to the Zn surface atoms [30] whereas the oxygen atoms in between appear lower in STM. The Zn lines in Fig. 1(b) are interrupted in five positions, which could be different types of vacancies [31]. The larger-scale color variations in this image are likely due to the incorporation of argon during sputtering.

At room temperature the resolution on ZnO($10\bar{1}0$) is generally lower compared to 400 K in our scanning tunneling microscope but the Zn lines can still be visible (data see Figure S.2). XPS performed on the as-prepared sample in UHV at room temperature and 400 K, respectively (data see Fig. 2), results in relative OH peak areas of 0.29 at room temperature and 0.07 at 400 K, whereas the relative area of the H_2O peak is 0.05 at room temperature and 0.04 at 400 K. Given the base pressure of $< 5 \cdot 10^{-9}$ mbar in the XPS chamber, the detected water and OH likely stem from the water background in the UHV. The amount of hydroxylation at 400 K is thus only 24 % of the amount of hydroxylation

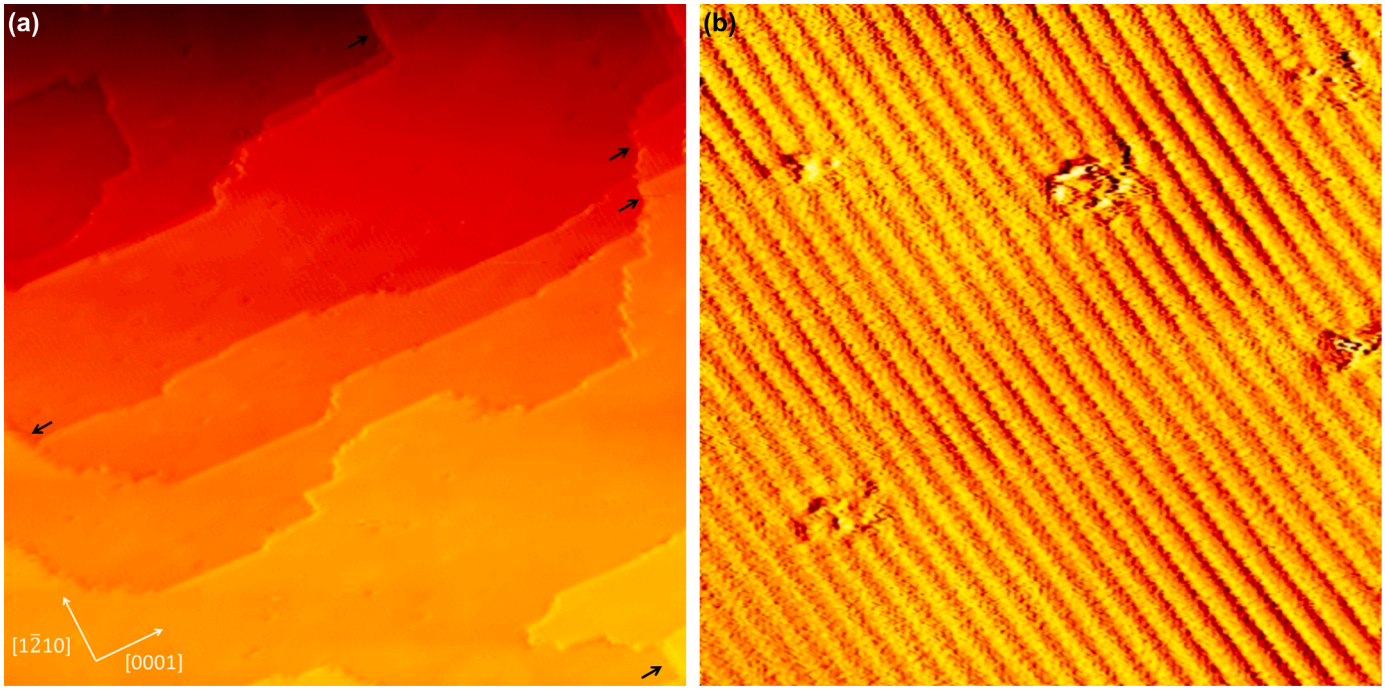

Fig. 1. (a) 80 nm x 80 nm STM image of the as-prepared ZnO($10\bar{1}0$) surface taken in UHV ($< 10^{-9}$ mbar) at 400 K with + 3 V and 50 pA. A plane filter image has been merged with the derivative. Black arrows mark double steps parallel to the [1$\bar{2}$10] direction. (b) 17 nm x 17 nm STM image of the same surface taken at 400 K with + 2.5 V and 50 pA. The plane filter was merged with the derivative in a ratio 2:1.

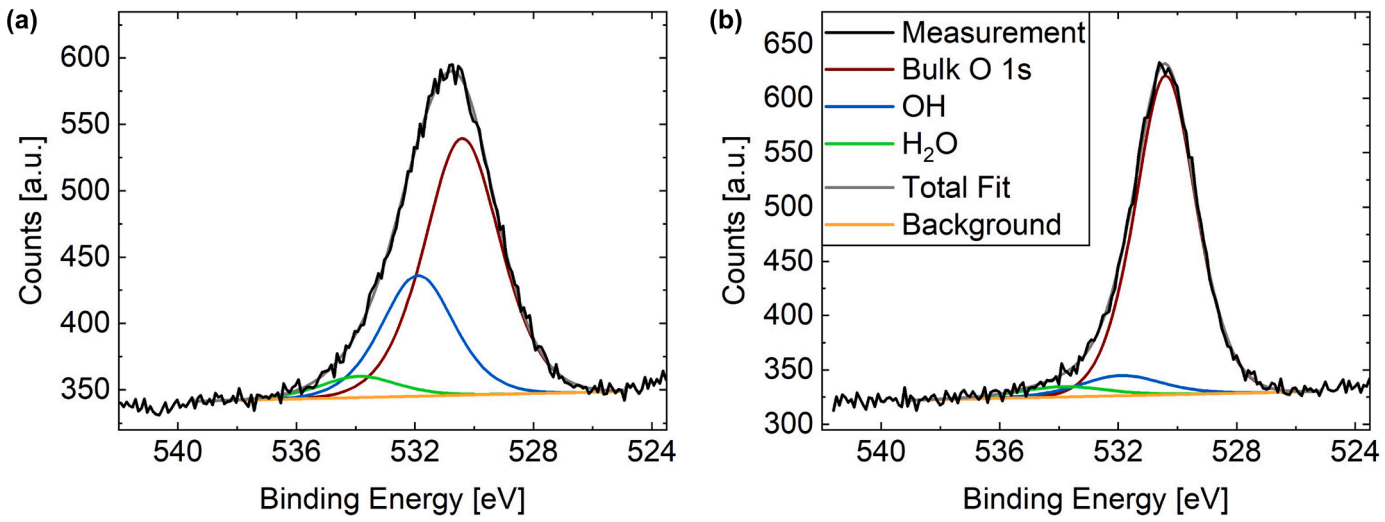

Fig. 2. Oxygen 1s spectra of the as-prepared ZnO($10\bar{1}0$) taken in UHV ($< 5 \cdot 10^{-9}$ mbar) at (a) 300 K and (b) 400 K. A linear background was subtracted and the fitted peaks are Gaussian-Lorentzian product functions with a ratio of 1:1. The details of the fitting procedure are described in the Methods Section.

at 300 K. Due to a partially overlapping Zn Auger peak with the O 1s peak, as described above, the XPS measurements are not suited to calculate absolute coverage values, but they show that more (partly dissociated) water is present on the surface at 300 K in comparison to 400 K. This is in agreement with the stability of the water overlayer up to about 370 K as observed by Meyer et al. [15]. That they do not observe the water overlayer at room temperature before deliberately dosing water into the UHV chamber could be explained by a difference in base pressure compared to the system used here.

The first water layer on ZnO($10\bar{1}0$) can be mobile and locally switch between a molecular and a half-dissociated layer as observed with scanning tunneling microscopy by Dulub et al. [14]. This can account for the more challenging scanning observed here at room temperature in comparison to 400 K. Following Ref. [28] it can be argued that the non-dissociated water in the first layer might rather contribute to the OH peak than the H_2O peak and it is, therefore, not possible to distinguish between the molecularly adsorbed and the half-dissociated first layer using XPS. However, we can detect the half-dissociated layer using low-energy electron diffraction at room temperature (data see Figure S.3).

3.2. *Rough phase of ZnO*(**$10\bar{1}0$**)

Fig. 3 shows the ZnO($10\bar{1}0$) surface after exposure to roughly 1 mbar of water for 10 min. The height profile in Fig. 3(b) shows a height difference between the terrace and the newly formed structure of between 0.23 nm and 0.33 nm. Although the accuracy of this value is limited by the ability of the tip to follow the rapid height change, the measured height difference is in agreement with the step height of ZnO($10\bar{1}0$) suggesting that the surface has roughened. This is confirmed by the stability of this phase in UHV for several days as well as the restructuring observed under annealing as depicted in Figure S.4. In order to restore the flatness of the as-prepared sample annealing to 795 K for 2 h is necessary.

The overview image of the rough surface in Fig. 3(c) allows for an estimation of the typical size of areas with the same height. In the [0001] direction the size is between 2 and 4 nm with some longer areas up to 7 nm mostly near the step edges. An example is marked with a yellow line. In the [$1\bar{2}10$] direction, however, the areas with the same height are up to 26 nm long. An example is marked with a blue line. This suggests that there is a clear favor for the formation of (0001)- or ($000\bar{1}$)-type steps, which are parallel to the [$1\bar{2}10$] direction, in comparison to the formation of ($1\bar{2}10$)-type steps, which are orthogonal to the [$1\bar{2}10$] direction. The original ($1\bar{2}10$)-type step edges in Fig. 3(c) show a roughly 2-nm-wide area without height difference as indicated by the grey arrows. This suggests that, although a large part of the terraces is elevated by one step height, double steps of this type are unfavored. On as-prepared surfaces with a large step density double steps of both types are present (see for example Fig. 1(a) in Ref. [32]. and Fig. 1(a) in Ref. [30].). However, on surfaces with lower step density we have observed more double steps in the parallel direction than the ($1\bar{2}10$) type. Examples of these double steps are marked with black arrows in Figs. 1(a), 3(c), and S.4(b). The ($1\bar{2}10$)-type of steps and double steps being unfavored suggests a lower stability of the ($1\bar{2}10$) face compared to the (0001) or ($000\bar{1}$) faces of ZnO. Although theory [33] suggests the opposite, ($1\bar{2}10$) is the least stable of the low-index faces according to experimental data [34]. This is confirmed by STM measurements showing that the ($1\bar{2}10$)-type step edge is the most active site for nucleation during the deposition of Cu on ZnO($10\bar{1}0$) [32].

Although the probability of formation of the two different types of steps and double steps during the roughening process in water can be motivated by the stability of the corresponding face, the total ratio of the two different types of single steps on the as-prepared surface does not agree with this difference in stability. The ratio of step types varies significantly with scanning position and in comparison to different publications as it additionally depends on other factors like the preparation procedure and the initial miscut of the single crystal.

3.3. *Hydroxylation and adsorbed water*

X-ray photoelectron spectroscopy measurements of the oxygen 1s peak have been taken after exposure to 1 bar argon containing about 1 mbar water. For technical reasons, the ZnO($10\bar{1}0$) surface has to be heated to 400 K in order to remove it from the reactor. Therefore, every XPS measurement was first done at this temperature and once more after cooling down to 300 K. An example fit is given in Fig. 2. With the main bulk oxygen peak fixed to 530.4 eV (following the procedure described in Ref. [16]) two more peaks are necessary for a satisfactory fit. Adsorbed OH is identified at a shift of + 1.4 eV to + 2.1 eV on the polar faces of ZnO [35,36] and at a shift of + 1.5 eV on the nonpolar faces like ZnO($10\bar{1}0$) [21,28]. With less literature values available molecularly adsorbed water might have a larger range of binding energy shifts between + 2.6 eV for the polar faces [35] and + 3.5 eV for the nonpolar faces [28]. Fixing the binding energy shifts to the same values of + 1.5 eV for OH and + 3.5 eV for H_2O for all measurements given here ensures

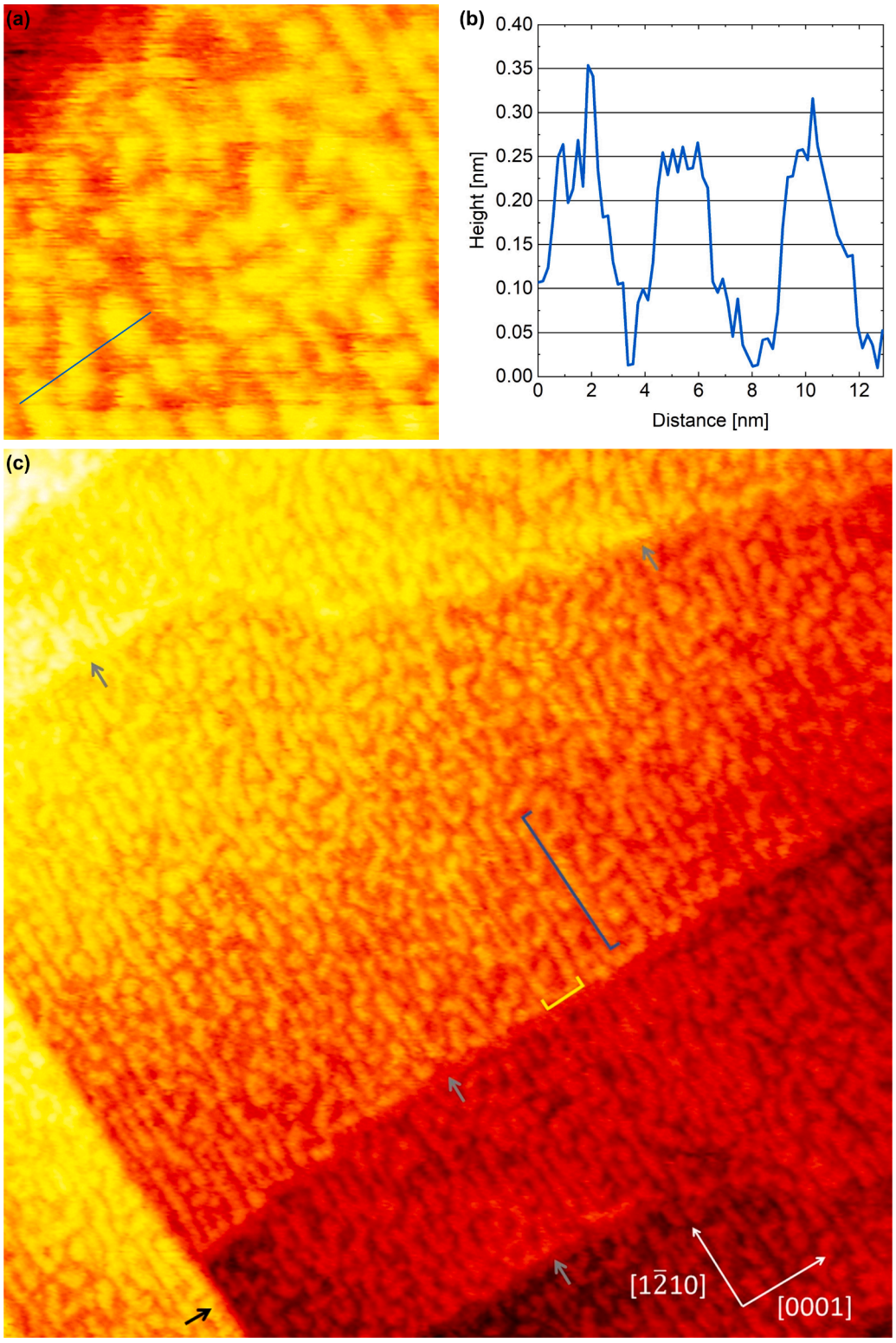

Fig. 3. (a) 35 nm x 35 nm STM image of ZnO(10$\bar{1}$0) after 10 min in roughly 1 mbar of water at room temperature with (b) the corresponding height profile. Including the initial filling of the reactor up to 1 bar of argon carrier gas the total exposure to the water flow is roughly 19 min (see experiment II in Figure S.5). (c) 150 nm x 150 nm STM image of ZnO(10$\bar{1}$0) under the same conditions. For better visibility of the steps as well as the structure on the terraces the plane filter image has been merged with its derivative at a ratio of 2:1. Examples of areas with the same height are marked with a blue line parallel to the [1$\bar{2}$10] direction and a yellow line parallel to the [0001] direction. A black arrow marks a (000$\bar{1}$)-type double step. Grey arrows mark (1$\bar{2}$10)-type steps accompanied by a 2-nm-wide area without height differences. Both STM images are taken in UHV at room temperature with + 3 V and 50 pA. (For interpretation of the references to colour in this figure legend, the reader is referred to the web version of this article.)

that the relative peak area values for the different situations can be compared. Details about the fitting method are given in Section 2. The relative areas of the OH as well as H_2O peaks, calculated as described in the Methods section, are used as a measure for the amount of hydroxylation and molecularly adsorbed water, respectively. By comparing multiple measurements taken after the same exposure (data not shown), the accuracy of the relative peak areas can be roughly estimated as ± 0.05. This value is taken into account in the following when interpreting the relative peak areas presented in Tables 1 and 2 for different exposures. Comparing all values taken at 400 K to the as-prepared surface at 400 K, the exposure to argon and therefore water does not increase the amount of hydroxylation within the detection limit of our instrumentation. Thus, no replacement of the OH on the surface by molecular water from the gas phase during exposure can be detected here. Letting the surface cool down to 300 K, the amount of hydroxylation increases for every measurement, however it does not reach the level measured on

Table 1
Relative OH peak areas for different exposure times, flows of water, and exposure temperatures in comparison to the as-prepared sample (in the first column) including XPS measurements taken at 400 K as well as at 300 K.

Exposure Time [min]	-	10	10	10	240
Flow [ml/min]	-	1	2	1	1
Exposure Temperature [K]	-	300	300	400	400
Relative OH peak area at 400 K	0.07	0.04	0.12	0.08	0.06
Relative OH peak area at 300 K	0.29	0.12	0.18	0.12	0.15

Table 2
Relative H_2O peak areas for different exposure times, flows of water, and exposure temperatures in comparison to the as-prepared sample (in the first column) including XPS measurements taken at 400 K as well as at 300 K.

Exposure Time [min]	-	10	10	10	240
Flow [ml/min]	-	1	2	1	1
Exposure Temperature [K]	-	300	300	400	400
Relative H_2O peak area at 400 K	0.04	0.1	0.12	0.16	0.14
Relative H_2O peak area at 300 K	0.05	0.08	0.09	0.13	0.09

the clean sample at 300 K. This could be due to a longer waiting time before taking the XPS spectra on the clean sample. After annealing to 800 K during the sample preparation, the surface takes longer to cool down from 400 K to 300 K, likely due to a higher temperature of surrounding parts on the sample holder. The higher amount of OH on the as-prepared sample could thus indicate that the hydroxylation increases over time in UHV ($< 5 \cdot 10^{-9}$ mbar). It is unlikely that the roughened surface is generally less active for water dissociation than the flat ZnO($10\bar{1}0$) as both ZnO(0001) [37] and ZnO($000\bar{1}$) [36] show dissociative water adsorption. However, it cannot be excluded that the larger amount of water present on the surface after an exposure (see next paragraph) leads to a slower hydroxylation process compared to on the as-prepared surface when cooling down from 400 K to 300 K. As will be discussed in Section 3.4, the adsorption structure and thus possibly dissociation behavior of the first adsorption layer is expected to differ depending on the amount of molecularly adsorbed water layers on top.

An increase in the H_2O relative peak area is detected right after the exposure in the measurements taken at 400 K compared to the clean sample at the same temperature. A part of this molecularly adsorbed water has desorbed when the XPS is measured at 300 K as can be seen in a decrease in the relative peak areas for all measurements. As the desorption of water cannot be caused by the decrease in temperature, this effect can only be attributed to the longer time passed since the end of the exposure. Given the accuracy of the relative peak areas of $\pm$ 0.05 the values measured at 300 K after exposure are comparable with the as-prepared surface. Thus, the desorption of the molecularly adsorbed water after the exposure proceeds faster than the increase in hydroxylation in UHV.

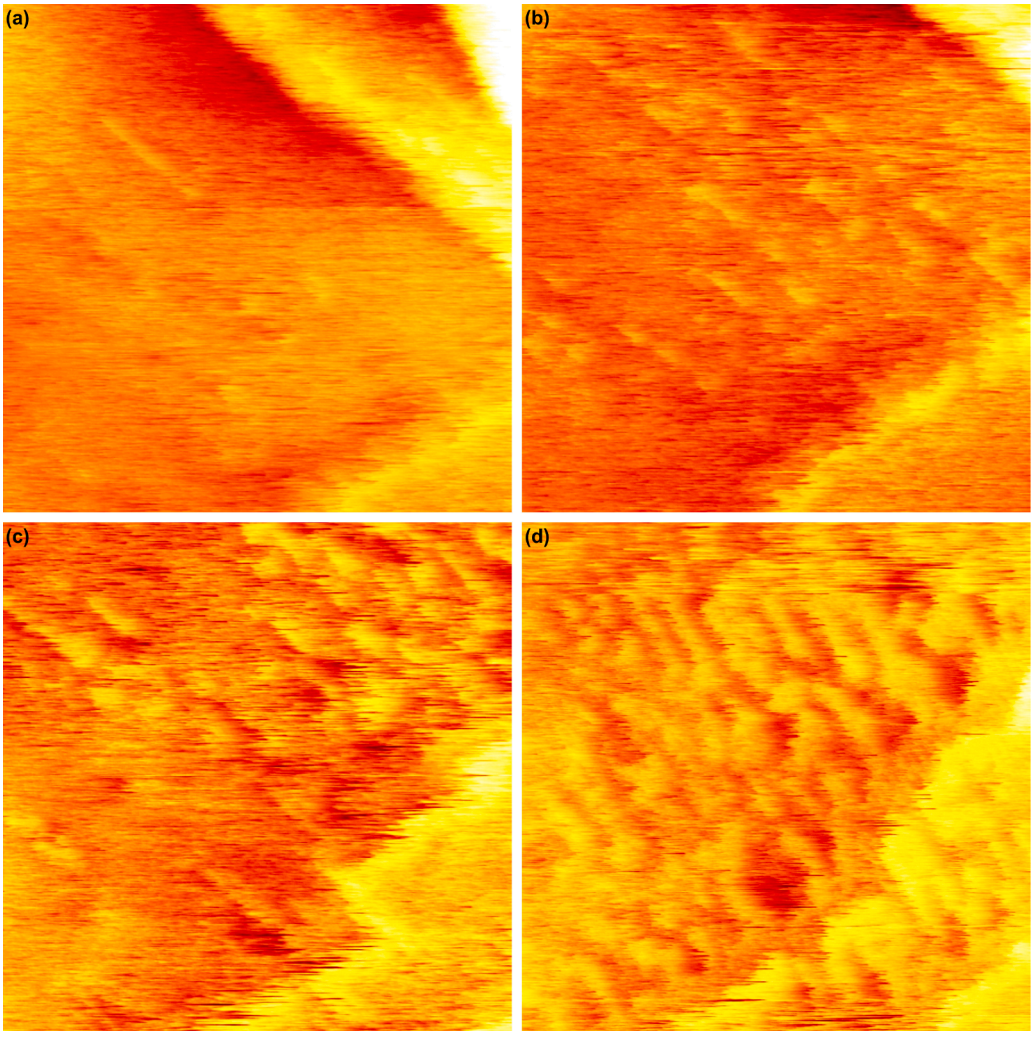

Fig. 4. 35 nm x 35 nm STM images of ZnO($10\bar{1}0$) in roughly 1 mbar of water at room temperature taken with + 2 V and 50 pA. The images were taken in situ (a) 13.0 min, (b) 14.2 min, (c) 16.7 min, and (d) 20.4 min after starting the flow of gas.

As the rough phase is stable in UHV at 300 K as well as 400 K, it can be concluded that, although the formation is induced by water, the presence of the rough phase is not directly correlated to the amount of hydroxylation and molecularly adsorbed water left on the surface after the end of the water exposure. This is additional evidence that the rough phase consists of zinc and oxygen atoms from the surface itself.

3.4. Roughening process

Fig. 4 shows the structural change of ZnO($10\bar{1}0$) in 1 bar of argon containing roughly 1 mbar of water. Comparing these STM images and corresponding heightlines to the measurements on the sample in UHV after such an exposure (see Section 3.2), the structural change can be identified as the roughening process. The XPS measurements in Section 3.3 suggest, however, that a larger amount of adsorbed water is present right after exposure which decreases over time in UHV. Therefore, a larger amount of adsorbed water could be present during the in situ measurements in Fig. 4 compared to the ex situ measurements in Fig. 3. The roughening process starts at multiple positions on the terrace and the surface is completely roughened 7.4 min afterwards. Figure S.5 compares two different measurements of the formation of the rough phase where different flows of carrier gas were used. It can be observed that the roughening starts earlier and proceeds faster when a higher flow is used even though the total pressure was lower at the onset of the roughening compared to the experiment with lower flow. This suggests that the water pressure is not the main factor that allows for the roughening of the surface and that a water pressure on the order of 0.1 mbar is sufficient as well.

Under prolonged exposure the ZnO($10\bar{1}0$) roughens more severely. Fig. 5(a) shows an STM image after 4 h in roughly 1 mbar of water. (For technical reasons this exposure was done at 400 K surface temperature.) As can be seen in the corresponding height profile in Fig. 5(b), the height difference on one terrace can be twice the step height of ZnO($10\bar{1}0$). Areas with a height difference of about 1.5 times the step height with respect to the lowest point on the terrace are observed as well. As one step consists of two layers of ZnO dimers, steps with about half the height can be observed when the topmost layer is missing. Apart from height differences that correspond to full or half steps, smaller height variations on the small terraces can be seen in Fig. 5(a). This suggests that the density of smaller vacancies increases as well. If they for example consist of only one missing dimer, they might not be resolved completely and therefore appear less deep than half the step height. Additionally, the surface could become increasingly amorphous with longer exposure and more severe restructuring. As vacancies can interact more strongly with water [38], the speed of the roughening process could increase over time.

Overall, we thus observe a restructuring of the ZnO($10\bar{1}0$) surface which must stem from an interaction with water that is significantly different from the interaction that leads to the ordered adsorption structures observed in UHV [14]. Theoretical studies on the interaction of ZnO($10\bar{1}0$) with water confirm that the 2x1 half-dissociated monolayer (with one dissociated and one molecular water molecule per two ZnO($10\bar{1}0$) unit cells) is the most stable structure in UHV [38–40]. However, the structure changes significantly when adding more water as investigated in detail by Kenmoe et al. [40]. From 3 monolayers on the first so-called contact layer is adsorbed on the surface in an ordered fashion while all additional water molecules are adsorbed in a "liquid-like film", which is more amorphous and can move between a number of different configurations. This picture of the water adsorption suggests that from 3 monolayers on the structure of the contact layer on the ZnO($10\bar{1}0$) surface does not change significantly when adding more water. This could account for our observation that the roughening does not primarily depend on the exact pressure in the 0.1 to 1 mbar regime investigated here. The dependence on the gas flow, however, could stem from the amount of water molecules that need to pass through the reactor before at least 3 monolayers are adsorbed and the contact layer is present. Tocci et al. [39] show that the properties of the contact layer lead to a significant increase in proton exchange to and from the surface in comparison to the 2x1 monolayer. Additionally, proton exchange between the dissociated and non-dissociated water molecules in the first layer, which is not possible in the 2x1 monolayer, occurs frequently in the contact layer. This proton mobility could be responsible for allowing

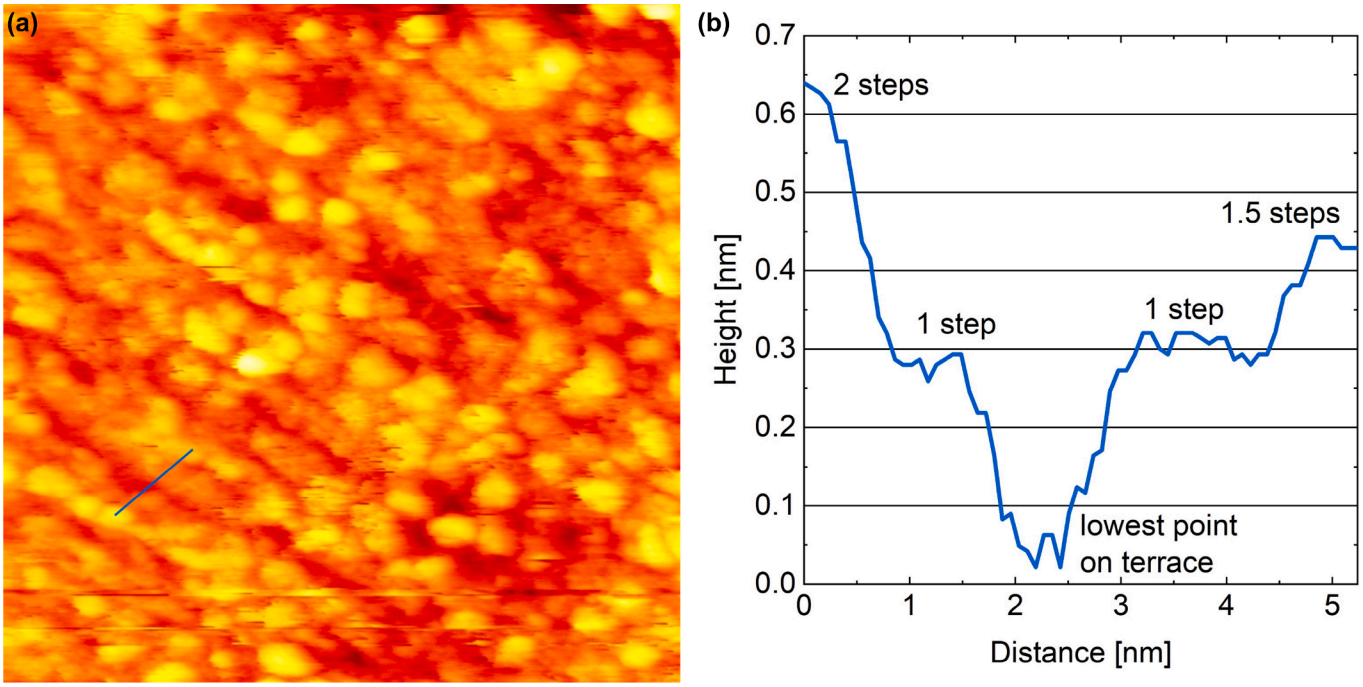

Fig. 5. (a) 35 nm x 35 nm STM image of ZnO($10\bar{1}0$) after 4 h in 1 mbar of water at 400 K with (b) the corresponding height profile indicated in blue. The image is taken in UHV at room temperature with + 4 V and 50 pA. (For interpretation of the references to colour in this figure legend, the reader is referred to the web version of this article.)

a restructuring of the ZnO($10\bar{1}0$) surface. A theoretical study by Kresse et al. [41] suggests a high reactivity of hydrogen with ZnO that can lead to the formation of OH from lattice oxygen and therefore to movement of oxygen atoms. A restructuring of the polar (0001) face of ZnO under the influence of water has been observed experimentally by Önsten et al. [37], confirming that water can induce mobility of zinc and oxygen atoms or the ZnO dimer. They observe a severe roughening of ZnO(0001) after a deposition of 20 L of water, which is explained as an interaction with hydrogen atoms from dissociated water as well. However, on the ZnO($10\bar{1}0$) face, although some vacancies are formed [30], no severe restructuring due to atomic hydrogen has been reported so far. Interestingly, before the (0001) surface roughens, the observations of Önsten et al. first show an increase in the size of the (0001) terraces under exposure to smaller amounts of water (up to 5 L). Thus, water itself, without a significant amount of leftover H atoms, might in turn stabilize the (0001) face. This is in agreement with calculations suggesting that adsorbed OH can stabilize ZnO(0001) [41]. This could explain the favored formation of (0001)-type steps observed here on ZnO($10\bar{1}0$) during the restructuring under the influence of water. The difference in stability of the different faces and step types, as observed in UHV [32,34], might thus be more severe in moderate pressures of water.

4. Conclusions

We have presented evidence for a significant roughening of the ZnO($10\bar{1}0$) surface in the 0.1 mbar to 1 mbar range of water, which proceeds within the first 10 min and is dependent on the total amount of water supplied to the surface. Hereby, the formation of (0001)- or ($000\bar{1}$)-type steps is favored over the formation of ($1\bar{2}10$)-type steps. This is discussed on the basis of their stability in UHV as well as in water background. For practical applications the water content in air as well as in industrially used gases is likely higher than in the mbar range, especially during reactions where water is a reactant or product. Thus, it can be assumed that the water content would be high enough for ZnO($10\bar{1}0$) to be present only in the rough phase at room temperature. This limits the applicability of UHV studies on ZnO($10\bar{1}0$) at room temperature as a model for methanol steam reforming catalysts as well as other ZnO devices. Additionally, the roughening could have influence on the interpretation of data taken at room temperature under elevated water pressures, such as near-ambient pressure XPS, where the surface is not imaged and assumed to be flat ZnO($10\bar{1}0$). Generally, although highly pure gases are usually used to ease the investigation of processes on the atomic level, our results exemplify that the presence of usual contaminants is a necessary part of moving towards more realistic conditions in in situ studies.

Declaration of Competing Interest

The authors declare the following financial interests/personal relationships which may be considered as potential competing interests:

Sabine Wenzel reports financial support was provided by BASF Nederland B.V. Sabine Wenzel reports financial support was provided by SABIC Global Technologies B.V. Sabine Wenzel reports financial support was provided by Sasol Technology (Pty) Ltd.

Acknowledgments

Funding: This work was supported by the Dutch Research Council (NWO), BASF Nederland B.V., SABIC Global Technologies B.V., and Sasol Technology (Pty) Ltd. [grant number 731.015.604].

Supplementary material

Supplementary material associated with this article can be found, in the online version, at 10.1016/j.susc.2021.121940

References

[1] Q.I. Roode-Gutzmer, D. Kaiser, M. Bertau, Renewable methanol synthesis, ChemBioEng Rev. 6 (6) (2019) 209–236, https://doi.org/10.1002/cben.201900012.
[2] J.H. Park, J.K. Park, Fate of methanol in an anaerobic digester, Korean J. Chem. Eng. 20 (3) (2003) 509–516, https://doi.org/10.1007/BF02705557.
[3] D.R. Lide, CRC Handbook of chemistry and physics, internet version 2005, CRC Press, Boca Raton, FL, 2005.www.hbcpnetbase.com
[4] B.A. Peppley, J.C. Amphlett, L.M. Kearns, R.F. Mann, Methanol-steam reforming on Cu/ZnO/Al_2O_3. Part 1: the reaction network, Appl. Catal., A 179 (1) (1999) 21–29, https://doi.org/10.1016/S0926-860X(98)00298-1.
[5] J. Larminie, A. Dicks, Fuel cell systems explained, John Wiley & Sons Ltd, Chichester, 2003.
[6] S. Sá, H. Silva, L. Brandão, J.M. Sousa, A. Mendes, Catalysts for methanol steam reforming-a review, Appl. Catal., B 99 (1–2) (2010) 43–57, https://doi.org/10.1016/j.apcatb.2010.06.015.
[7] X. Xu, K. Shuai, B. Xu, Review on copper and palladium based catalysts for methanol steam reforming to produce hydrogen, Catalysts 7 (6) (2017) 183, https://doi.org/10.3390/catal7060183.
[8] A. Iulianelli, P. Ribeirinha, A. Mendes, A. Basile, Methanol steam reforming for hydrogen generation via conventional and membrane reactors: a review, Renewable Sustainable Energy Rev. 29 (January) (2014) 355–368, https://doi.org/10.1016/j.rser.2013.08.032.
[9] H. Lorenz, M. Friedrich, M. Armbrüster, B. Klötzer, S. Penner, ZnO is a CO_2-selective steam reforming catalyst, J Catal 297 (2013) 151–154, https://doi.org/10.1016/j.jcat.2012.10.003.
[10] Y. Matsumura, H. Ishibe, Suppression of CO by-production in steam reforming of methanol by addition of zinc oxide to silica-supported copper catalyst, J Catal 268 (2) (2009) 282–289, https://doi.org/10.1016/j.jcat.2009.09.026.
[11] X. Shao, K.-i. Fukui, H. Kondoh, M. Shionoya, Y. Iwasawa, STM Study of surface species formed by methanol adsorption on stoichiometric and reduced ZnO($10\bar{1}0$)surfaces, J. Phys. Chem. C 113 (2009) 14356–14362, https://doi.org/10.1021/jp9022597.
[12] J. Kiss, D. Langenberg, D. Silber, F. Traeger, L. Jin, H. Qiu, Y. Wang, B. Meyer, C. Wöll, Combined theoretical and experimental study on the adsorption of methanol on the ZnO($10\bar{1}0$) surface, J. Phys. Chem. A 115 (25) (2011) 7180–7188, https://doi.org/10.1021/jp200146v.
[13] L. Jin, Y. Wang, Surface chemistry of methanol on different ZnO surfaces studied by vibrational spectroscopy, PCCP 19 (20) (2017) 12992–13001, https://doi.org/10.1039/c7cp01715d.
[14] O. Dulub, B. Meyer, U. Diebold, Observation of the dynamical change in a water monolayer adsorbed on a ZnO surface, Phys. Rev. Lett. 95 (13) (2005) 1–4, https://doi.org/10.1103/PhysRevLett.95.136101.
[15] B. Meyer, D. Marx, O. Dulub, U. Diebold, M. Kunat, D. Langenberg, C. Wöll, Partial dissociation of water leads to stable superstructures on the surface of zinc oxide, Angewandte Chemie - International Edition 43 (48) (2004) 6642–6645, https://doi.org/10.1002/anie.200461696.
[16] C. Wöll, The chemistry and physics of zinc oxide surfaces, Prog Surf Sci 82 (2007) 55–120, https://doi.org/10.1016/j.progsurf.2006.12.002.
[17] Z. Li, H. Shi, H. Yuan, S. Ruan, W. Wang, Z. Li, X. Shao, Adsorption and diffusion of CO on clean and CO_2-Precovered ZnO($10\bar{1}0$), J. Phys. Chem. C 122 (16) (2018) 8919–8924, https://doi.org/10.1021/acs.jpcc.8b00039.
[18] M. Buchholz, X. Yu, C. Yang, S. Heißler, A. Nefedov, Y. Wang, C. Wöll, IR-spectroscopy of CO adsorption on mixed-terminated ZnO surfaces, Surf Sci 652 (2016) 247–252, https://doi.org/10.1016/j.susc.2015.12.029.
[19] H. Shi, S. Ruan, H. Liu, L. Wang, W. Wang, X. Ren, B. Wang, K. Wu, X. Shao, Directional growth of one-Dimensional CO_2chains on ZnO($10\bar{1}0$), J. Phys. Chem. C 120 (41) (2016) 23669–23674, https://doi.org/10.1021/acs.jpcc.6b08358.
[20] R. Lindsay, G. Thornton, Structure of atomic and molecular adsorbates on low-Miller-Index ZnO surfaces using X-ray absorption spectroscopy, Top. Catal. 18 (1–2) (2002) 15–19, https://doi.org/10.1023/A:1013821915062.
[21] J.T. Newberg, C. Goodwin, C. Arble, Y. Khalifa, J.A. Boscoboinik, S. Rani, ZnO($10\bar{1}0$) Surface hydroxylation under ambient water vapor, J. Phys. Chem. B 122 (August 2017) (2018) 472–478, https://doi.org/10.1021/acs.jpcb.7b03335.
[22] C.T. Herbschleb, P.C.V.D. Tuijn, S.B. Roobol, V. Navarro, J.W. Bakker, Q. Liu, D. Stoltz, G. Verdoes, M.A.V. Spronsen, M. Bergman, L. Crama, I. Taminiau, A. Ofitserov, G.J.C.V. Baarle, J.W.M. Frenken, The reactorstm: atomically resolved scanning tunneling microscopy under high-pressure, high-temperature catalytic reaction conditions, Rev. Sci. Instrum. 85 (2014) 083703, https://doi.org/10.1063/1.4891811.
[23] M.J. Rost, L. Crama, P. Schakel, E. van Tol, G.B.E.M. van Velzen-Williams, C. F. Overgauw, H. ter Horst, H. Dekker, B. Okhuijsen, M. Seynen, A. Vijftigschild, P. Han, A.J. Katan, K. Schoots, R. Schumm, W. van Loo, T.H. Oosterkamp, J.W. M. Frenken, Scanning probe microscopes go video rate and beyond, Rev. Sci. Instrum. 76 (5) (2005) 053710, https://doi.org/10.1063/1.1915288.
[24] https://secure.eld.leidenuniv.nl/~moene/software/camera/Camera/Camera-MainPage.html.
[25] I. Horcas, R. Fernández, J.M. Gómez-Rodríguez, J. Colchero, J. Gómez-Herrero, A. M. Baro, WSXM: A software for scanning probe microscopy and a tool for nanotechnology, Rev. Sci. Instrum. 78 (1) (2007) 013705, https://doi.org/10.1063/1.2432410.

[26] Product information provided by Westfalen: www.westfalengassen.nl/industriele-gassen/alle-gassen-op-een-rij/applicationdetailviewnl/productdetailviewnl/gas/argon-50-5.html, accessed on 22.08.2019.
[27] M.A.v. Spronsen. Oxidation catalysis on Pt and Au : complexity of simple chemistry, Leiden University, 2016. Ph.D. thesis.
[28] R. Heinhold, S.P. Cooil, D.A. Evans, M.W. Allen, Stability of the surface electron accumulation layers on the nonpolar $(10\bar{1}0)$ and $(11\bar{2}0)$faces of ZnO, The Journal of Physical Chemistry C 118 (42) (2014) 24575–24582, https://doi.org/10.1021/jp507820m.
[29] H. Morkoc, U. Özgür, General properties of ZnO, Wiley-VCH Verlag GmbH & Co. KGaA, 2009, https://doi.org/10.1002/9783527623945.ch1.
[30] X.L. Yin, A. Birkner, K. Hänel, T. Löber, U. Köhler, C. Wöll, Adsorption of atomic hydrogen on ZnO$(10\bar{1}0)$: STM study, PCCP 8 (13) (2006) 1477–1481, https://doi.org/10.1039/b515464b.
[31] R. Kováčik, B. Meyer, D. Marx, F centers versus dimer vacancies on ZnO surfaces: characterization by STM and STS calculations, Angewandte Chemie - International Edition 46 (26) (2007) 4894–4897, https://doi.org/10.1002/anie.200604399.
[32] O. Dulub, L.A. Boatner, U. Diebold, STM study of Cu growth on the ZnO$(10\bar{1}0)$ surface, Surf Sci 504 (2002) 271–281, https://doi.org/10.1016/S0039-6028(02)01107-X.
[33] B. Meyer, D. Marx, Density-functional study of the structure and stability of ZnO surfaces, Physical Review B - Condensed Matter and Materials Physics 67 (3) (2003) 1–11, https://doi.org/10.1103/PhysRevB.67.035403.
[34] L. Boatner, U. Diebold, O. Dulub, STM study of the geometric and electronic structure of ZnO(0001)-Zn, $(000\bar{1})$-O, $(10\bar{1}0)$, and $(11\bar{2}0)$ surfaces, Surf Sci 519 (July 2014) (2002) 201–217, https://doi.org/10.1016/S0039-6028(02)02211-2.
[35] R. Heinhold, G.T. Williams, S.P. Cooil, D.A. Evans, M.W. Allen, Influence of polarity and hydroxyl termination on the band bending at ZnO surfaces, Physical Review B - Condensed Matter and Materials Physics 88 (23) (2013), https://doi.org/10.1103/PhysRevB.88.235315.
[36] M. Kunat, S.G. Girol, U. Burghaus, C. Wöll, The interaction of water with the oxygen-terminated, polar surface of ZnO, The Journal of Physical Chemistry B 107 (51) (2003) 14350–14356, https://doi.org/10.1021/jp030675z.
[37] A. Önsten, D. Stoltz, P. Palmgren, S. Yu, M. Göthelid, U.O. Karlsson, Water adsorption on ZnO(0001): transition from triangular surface structures to a disordered hydroxyl terminated phase, J. Phys. Chem. C 114 (25) (2010) 11157–11161, https://doi.org/10.1021/jp1004677.
[38] A. Calzolari, A. Catellani, Water adsorption on nonpolar ZnO$(10\bar{1}0)$ surface: a microscopic understanding, J. Phys. Chem. C 113 (7) (2009) 2896–2902, https://doi.org/10.1021/jp808704d.
[39] G. Tocci, A. Michaelides, Solvent-induced proton hopping at a water-oxide interface, J. Phys. Chem. Lett. 5 (3) (2014) 474–480, https://doi.org/10.1021/jz402646c.
[40] S. Kenmoe, P. Ulrich Biedermann, Water aggregation and dissociation on the ZnO$(10\bar{1}0)$ surface, PCCP 19 (2) (2017) 1466–1486, https://doi.org/10.1039/c6cp07516a.
[41] G. Kresse, O. Dulub, U. Diebold, Competing stabilization mechanism for the polar ZnO(0001)-Zn surface, Physical Review B - Condensed Matter and Materials Physics 68 (24) (2003) 1–15, https://doi.org/10.1103/PhysRevB.68.245409.